Structural studies of tropomyosin by cryoelectron microscopy and x-ray diffraction

Donna Cabral-Lilly,* George N. Phillips, Jr.,‡ Gina E. Sosinsky,* Linda Melanson,* Susan Chacko,‡§ and Carolyn Cohen*

*Rosenstiel Basic Medical Sciences Research Center, Brandeis University, Waltham, Massachusetts 02254-9110; ‡Department of Biochemistry, Rice University, Houston, Texas 77251; and §Graduate Program in Biophysics, University of Illinois at Urbana-Champaign, Urbana, Illinois 61801 USA

ABSTRACT A comparison has been made between cryoelectron microscope images and the x-ray structure of one projection of the Bailey tropomyosin crystal. The computed transforms of the electron micrographs extend to a resolution of ~ 18 Å compared with the reflections from x-ray crystallography which extend to 15 Å. After correction of the images for lattice distortions and the contrast transfer function, the structure factors were constrained to the plane group (*pmg*) symmetry of this projection. Amplitude and phase data for five images were compared with the corresponding view from the three-dimensional x-ray diffraction data (Phillips, G. N., Jr., J. P. Fillers, and C. Cohen. 1986. *J. Mol. Biol.* 192:111–131). The average *R* factor between the electron microscopy and x-ray amplitudes was 15%, with an amplitude-weighted mean phase difference of 4.8°. The density maps derived from cryoelectron microscopy contain structural features similar to those from x-ray diffraction: these include the width and run of the filaments and their woven appearance at the crossover regions. Preliminary images obtained from frozen-hydrated tropomyosin/troponin cocrystals suggest that this approach may provide structural details not readily obtainable from x-ray diffraction studies.

INTRODUCTION

Methods for low temperature transmission electron microscopy (cryo-EM) and image processing have now been developed that allow proteins and other biological macromolecules to be studied without the addition of heavy metal stains by embedding in vitreous ice or in glucose or other sugars. Using these techniques, the structures of protein microcrystals, two-dimensional arrays and single particles have been solved to moderate resolutions (7–20 Å) (for review see Glaeser, 1985; Chiu, 1986). A small number of proteins embedded in sugars have been solved to high resolution (e.g., bacteriorhodopsin, Henderson et al., 1990; and PhoE porin, Jap et al., 1990). There are several technical difficulties, however, in obtaining high resolution structural information by cryo-EM. Electron diffraction provides accurate Fourier amplitudes at high resolution for well-ordered areas containing large numbers of unit cells; for less ordered specimens or for single particles, however, structural information must be obtained from electron images. In addition, processing of the electron images includes corrections for imperfections and properties of the microscope lenses (e.g., the contrast transfer function [CTF]), and for disorder and/or distortions in the protein arrays. Many of the parameters used in these corrections, however, are estimates for experimental conditions that are difficult to determine precisely without knowing the solved structure. Comparison with x-ray diffraction data, when available, may be useful in determining initial estimates of underfocus for correcting the cryo-EM images as illustrated for tobacco mosiac virus (Jeng et al., 1989), and also provides an independent reference for checking the accuracy of the structural information determined from image analysis. The physical basis of the scattering is obviously different in the two techniques, but for biological specimens at low resolution the images should be very similar. In this paper we report a detailed comparison of a protein crystal structure determined by x-ray diffraction and cryo-EM of crystals in vitreous ice which illustrates the results of several different methods used for image processing cryo-EM micrographs. Tropomyosin is especially suitable for this kind of study: this protein forms crystals of a size and morphology amenable to analysis by both techniques.

Tropomyosin is a 400 Å long, α-helical, coiled–coiled protein; together with troponin, it forms a calcium-sensitive regulatory switch in many muscles. The classical, highly hydrated (> 95% solvent) tropomyosin Bailey crystal is made up of supercoiled filaments similar in structure to those that wind around the actin filaments in muscle (Caspar et al., 1969; Phillips et al., 1979, 1986). Models derived from electron micrographs of the [0kl] projection of negatively stained crystals (Caspar et al., 1969; Cohen et al., 1971) were critical in the solution of this projection of the lattice by x-ray diffraction. Additional modeling and solvent leveling techniques were used to solve the three-dimensional structure to 15 Å resolution (Phillips et al., 1986). (A different crystal form of tropomyosin that diffracts to ~ 5 Å has recently been produced but the structure has not yet been solved

0006-3495/91/04/805/10 $2.00

by x-ray crystallography [Stewart, 1984; Phillips et al., 1987].) We present here a comparison of the structure of the [0kl] projection of the tropomyosin Bailey crystal determined by cryo-EM with that derived from x-ray diffraction. We also present preliminary cryo-EM results of tropomyosin/troponin cocrystals which show features of the complex not readily seen by x-ray diffraction.

MATERIALS AND METHODS

Protein preparation and crystallization

α_2 tropomyosin (or $\alpha\alpha$ [Lehrer, 1975]) was purified from rabbit cardiac muscle, and unfractionated tropomyosin (α_2 plus $\alpha\beta$) was isolated from rabbit psoas muscle as described by Phillips et al. (1979). Troponin was prepared from the rabbit psoas muscle by a modification of the procedure of Greaser and Gergely (1973) as described by White et al. (1987). The proteins were stored in lyophilized form, and hydrated in 0.6 M KCl, 50 mM Tris-HCl, pH 8.0, 1 mM dithiothreitol (DTT) (0.5 mM $CaCl_2$ included for all troponin solutions). The hydrated proteins were dialyzed against a precrystallization buffer of 0.03 M sodium acetate, 0.05 M ammonium sulfate, 1 mM DTT, pH 6.2. All procedures were done at 4°C.

Tropomyosin crystallites suitable for electron microscopy (EM) were grown at a protein concentration of 3–4 mg/ml by two methods. In one crystallization procedure (a modification of the method of Caspar et al., 1969), a solution of tropomyosin (cardiac or unfractionated skeletal protein) was dialyzed against 0.01 sodium acetate, 0.05 M ammonium sulfate, 1 mM DTT, pH 5.6, with stirring. Crystals formed over 3–4 d and typically were rhomboid in shape with dimensions in the range of 0.3–0.5 μm. In the second method, crystals were grown by a modification of the method of Greaser et al. (1977). The protein solution was dialyzed against 0.2 M KCl, 0.01 M sodium acetate, 1 mM DTT, pH 5.6, with stirring. Rectangular- and rhomboid-shaped crystals grew in 4–6 d. Most of the crystals grown from pure α_2 tropomyosin, using either procedure, had a double-mesh lattice (Greaser et al., 1977). Crystals grown from the unfractionated skeletal tropomyosin were consistently of the single-mesh Bailey form and were therefore used for further analysis. These crystals were ~3–5 unit cells thick.

Reconstituted relaxing factor was made by mixing tropomyosin and troponin in solution at molar ratios of 1.0:1.0–1.5, at a total protein concentration of 4–6 mg/ml before the precrystallization dialysis. Cocrystals were formed by a modification of the method of Higashi and Ooi (1968). The complex was dialyzed against 0.36 M KCl, 0.01 M sodium acetate, 0.5 mM $CaCl_2$, 1 mM DTT, pH 5.3, with stirring. Small rectangular crystals formed in 7–14 d.

Electron microscopy

For microscopy of unstained crystals in vitreous ice, a sample was adsorbed to a 400 mesh copper grid coated with a holey carbon film for 2–3 min. The sample was blotted with filter paper to a thin film and quickly frozen by plunging into liquid propane cooled to liquid nitrogen temperature (Dubochet et al., 1988). The grids were viewed on a model EM420T transmission electron microscope (Philips Electronic Instruments, Inc., Mahwah, NJ) equipped with a model 651N anticontaminator and a model 626 cryoholder (Gatan, Inc., Warrendale, PA) cooled to −172°C. A Philips Electronic Instruments, Inc. low dose kit was used to record micrographs at a magnification of 47,000–48,000 of crystal fragments suspended in vitreous ice over holes (total electron dose ~$10e^-/Å^2$). Negatively stained samples of the tropomyosin crystals were prepared on carbon-coated 400 mesh copper grids as previously described (Caspar et al., 1969). Low dose electron micrographs were recorded at ambient temperature.

Image processing

Images of unstained tropomyosin crystals were screened by optical diffraction (Salmon and DeRosier, 1981). Areas whose diffraction patterns showed low amounts of drift and astigmatism, high degrees of symmetry, and resolution that extended to ~25 Å or better were selected for further processing. The images were digitized using a model P1000 (Optronics International, Inc., Chelmsford, MA) scanner at a 25μm raster step corresponding to 5.3 Å per pixel.

The underfocus of selected micrographs was estimated from the Thon rings from an area of carbon adjacent to the crystal. No further refinement of the defocus value was carried out. Lattice distortions were corrected by real space correlation analysis with unbending (Henderson et al., 1986) or by rotational alignment with unbending (Schmid, M., personal communication). For real space correlation analysis, the digitized image was processed by Fourier methods to remove low and high frequency noise and to locally average adjacent unit cells within the image (Sosinsky et al., 1990). A reference area consisting of one asymmetric unit (one "kite") was chosen from the most uniform area of the least distorted filtered image. The cross-correlation maps between the reference area and the unfiltered boxed images were calculated. Allowing a 5% error limit from the ideal unit cell, lattice distortion corrections were calculated and applied, and an averaged, unbent image of a single asymmetric unit was produced. This image was spliced to a larger array, and the Fourier transform calculated and indexed for each unbent image. Structure factors were extracted as described by Henderson et al. (1986). The phase origin was refined to the best twofold axis to preserve the plane group (*pmg*) symmetry. The average mean phase difference for the five images was 31.3°, with a weighted difference of 10.3°.

For the rotational alignment with unbending procedures, nontranslational disorder was corrected by modeling it as rotational disorder. The displacement vectors (the difference between lattice-predicted position and actual position) were found for each of the cross-correlation peaks. A consistent change in the size of the displacement vectors was taken as evidence of rotation. The image was then reinterpolated to correct for the translational and rotational disorder simultaneously, and the structure factors derived and corrected as described above.

Both sets of structure factors were corrected for the effects of the CTF by using the defocus estimated from the Thon rings according to the equation given by Erikson and Klug (1971). The fraction of amplitude contrast was determined empirically by trial and error using the *R*-factor obtained by comparing the x-ray amplitudes to those from the EM images as the criterion. This fraction is strongly determined by the very low resolution terms, and did not vary significantly from one image to the next. Once the CTF corrections were applied, plots were constructed (Wilson, 1949) using the ratio of the x-ray to the EM-derived structure factor amplitudes to indicate the relative difference in disorder in the two types of data. The slope of such a plot yields the Debye-Waller temperature factor required to cause the same resolution fall-off in the two sets of intensity data. The temperature factor could be applied to the x-ray data to lower their resolution to that of the EM data or, as we have done, an inverse temperature factor can be applied to enhance the higher order terms of the EM data to match more closely the resolution of the x-ray data. The poor signal-to-noise ratio of the weak high resolution EM structure factors limits the ability to scale them accurately to the x-ray values, resulting in variations in the flat solvent region as well as in the protein region. For the purpose of comparison, intermediate temperature factors

were therefore applied to the EM data that increase the apparent resolution without adding excessive noise in the solvent region.

For the tropomyosin/troponin cocrystals, partial occupancy and disorder of the troponin in the lattice occurs. Averages of the tropomyosin/troponin complex were therefore produced by a modified correlation averaging procedure for lattices containing variable substructure (Sosinsky et al., 1990). The final map (produced from the addition of 150 unit cells) was spliced to a larger area and processed as described for the tropomyosin crystals.

Comparison of x-ray and EM results

For comparison with the electron micrographs, the plane of diffraction data corresponding to the projection of the structure along the [0kl] axis was extracted from the three-dimensional x-ray data set. The phases of the data set were then shifted to move one of the twofold axes to the origin, such that the two-dimensional space group *pmg* was conserved. It was also necessary to invert the contrast of the image by applying a phase shift of 180° to the x-ray phases to match the EM data.

The *R* factor between EM and x-ray data was calculated for each image as follows:

$$R = \sum_{kl} \left| F_{em} - F_{xray} \right| / \sum_{kl} F_{xray}.$$

The mean phase differences were calculated as:

$$\left(\text{Mean phase difference} = \sum_{kl} wt_{kl} \left| \text{PHASE}_{em} - \text{PHASE}_{xray} \right| / \sum wt_{kl}\right)$$

Unweighted phase differences were calculated with $wt_{kl} = 1$, and weighted phase differences with wt_{kl} set to the x-ray amplitude for that reflection. For the purpose of comparing the different distortion-correction methods, only common reflections for the data sets from all methods were used in the statistics, typically 250–300 reflections for each image.

RESULTS

Qualitative comparison of images of frozen-hydrated and negatively stained crystals with x-ray diffraction results

There are striking differences between images of frozen-hydrated and negatively stained tropomyosin Bailey crystallites. The images of the [0kl] projection of ice-embedded crystal fragments show remarkable contrast, and the density distribution along the filaments is relatively uniform with only a slight increase at the crossovers in the unprocessed image (Fig. 1 *a*). In areas of some micrographs, separation of the two coiled–coiled filaments can be clearly seen, as well as the woven appearance of the crossover regions (see Fig. 1 *a*, *inset*). These areas closely resemble the arrangement of tropomyosin molecules for this projection of the crystal lattice determined from x-ray diffraction studies (Fig. 1 *c*; Phillips et al., 1986). In contrast, when negative staining is used, the images are dominated by a pattern of bright nodes at the crossover regions separated by weak, relatively indistinct, strands of filaments (Caspar et al., 1969; see Fig. 1 *b*). The crossover regions are especially accentuated because of the high density of protein in this region, and because the filaments at the crossovers are more ordered than the intervening strands (Phillips et al., 1980). Occasionally, separation between the coiled-coil filaments in the strands can be seen, but these appear disordered and are relatively indistinct. Correspondingly, the characteristic spikes of intensity in the diffraction pattern, which arise from the tropomyosin filaments in the lattice, are evident in the transform of the cryo-EM image, but not in the transform from the negatively stained crystallite (Fig. 1 *d–f*). The *pmg* symmetry of this projection is preserved, however, in both the frozen-hydrated and negatively stained crystallites. The computed diffraction pattern of the cryo-EM micrograph extends to 18 Å and is slightly lower in resolution than the 15 Å data achieved by x-ray diffraction; the negatively stained image diffracts to only 30 Å, even when low electron doses are used. The unit cell parameters obtained using the two techniques are also comparable and are similar to those of the x-ray crystals, but there is greater variation between images of the stained preparations. Despite the lack of correspondence in a number of aspects with the x-ray diagrams, images of the negatively stained crystallites provided a model that was critical for solving the projected structure by x-ray diffraction (Caspar et al., 1969; Cohen et al., 1971; Phillips et al., 1979). In contrast, the images of the ice-embedded crystals may be used to determine directly the projected crystal structure for comparison with the x-ray results.

Detailed comparison between cryoelectron microscopy and x-ray diffraction results

Various corrections have been applied to the images from cryo-EM, and the resulting density maps and extracted structure factors compared with the known x-ray structure at 15 Å resolution. Table 1 shows a quantitative comparison of the Fourier transforms of the EM images with the x-ray images for each stage of the analysis. The crystallographic *R* factor, overall mean phase difference, a Debye-Waller temperature factor relative to the x-ray data, and an amplitude-weighted mean phase difference are reported for five EM images and the average of these images. The amplitude-weighted term is included to indicate the degree to which the phases of the strong reflections are in agreement. For comparison, it should be pointed out that the symmetry-constrained phases in this projection are cen-

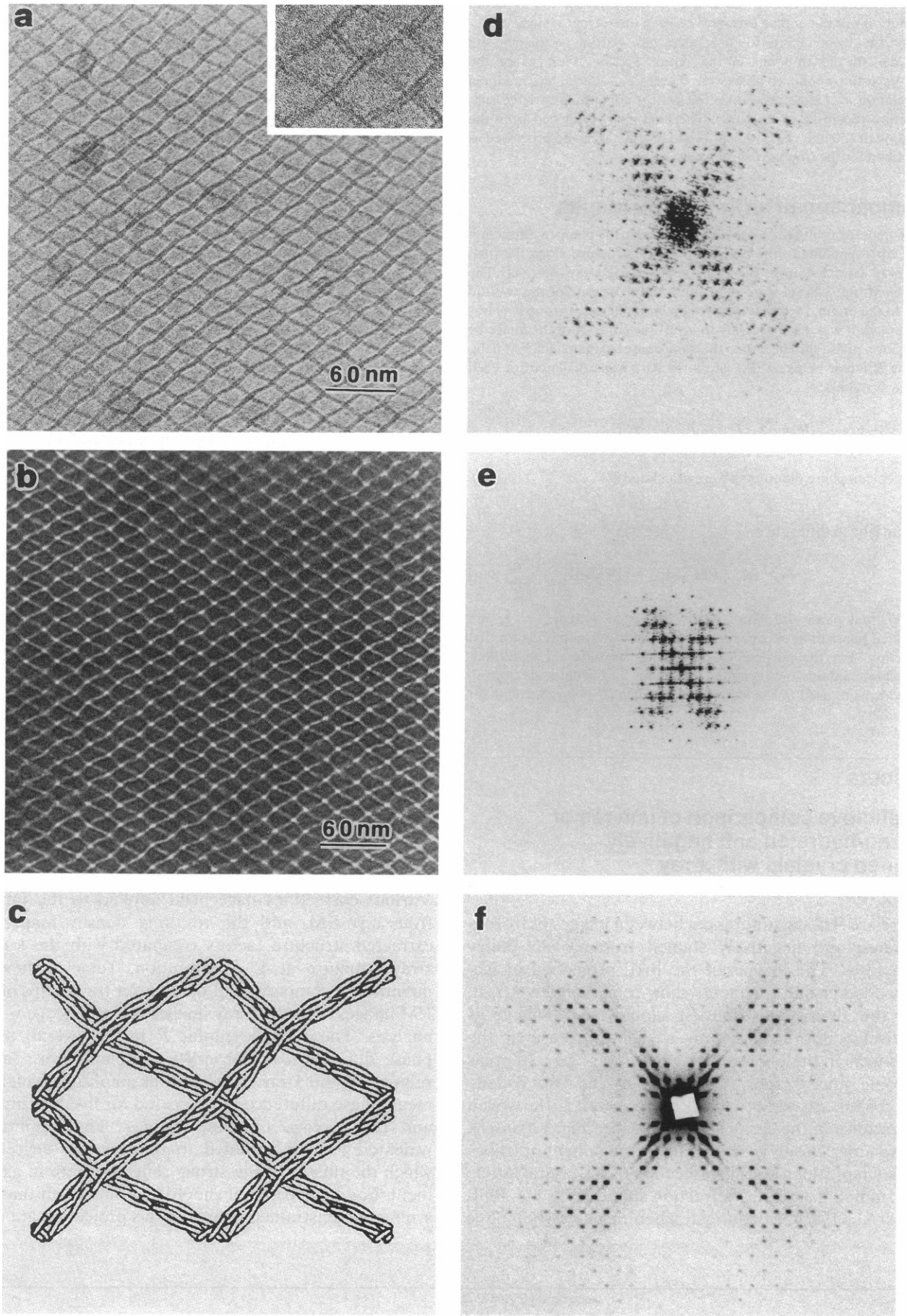
a
60 nm
d
b
60 nm
e
c
f

TABLE 1 **Comparison of structure factors from cryo-EM and x-ray diffraction***

Image #	Average displacement from ideal lattice	Unrefined image‡			No lattice corrections§			Unbending/unrotating§			Unbending/selected average§			Temperature factor‖
		R	Mean phase difference		*R*	Mean phase difference		*R*	Mean phase difference		*R*	Mean phase difference		
	Å	%	*NW*	*W*	%	*NW*	*W*	%	*NW*	*W*	%	*NW*	*W*	Å²
1	9.3	51	66	34	14	52	9.2	15	58	8.6	20	59	7.8	6,011
2	14.8	44	67	37	16	57	7.8	16	50	6.2	15	57	6.0	8,688
3	4.2	37	65	37	19	41	2.1	19	44	2.7	20	44	3.3	8,462
4	9.0	38	52	24	19	39	3.9	16	42	3.4	18	40	4.4	8,953
5	5.0	30	64	26	11	45	1.5	11	42	1.6	12	49	2.3	10,738
Average	8.5	40	63	31	16	47	4.9	15	47	4.5	17	50	4.8	8,489

*R factor and mean phase difference determined using cryo-EM-derived structure factors before and after lattice distortion corrections as indicated; ‡*NW* = unweighted; *W* = weighted phase difference; §*pmg* symmetry, CTF correction and temperature factor applied to cryo-EM structure factors; ‖average of temperature factors from Wilson plots derived from each of the distortion-corrected data sets.

trosymmetric and that two random distributions of phases would have a mean difference of 90°. Fig. 2 *a–f* shows density maps derived from the EM structure factors, for image 1 of Table 1, after each correction, as well as an electron density map derived from the x-ray diffraction data.

Initial comparisons of the EM and x-ray data were made without enforcing the *pmg* symmetry and without any other corrections. The phases of the EM images were refined to the best origin to preserve the symmetry of this projection, and the various factors described above were calculated. The *R* factors for the five images when compared with the x-ray data ranged from 30 to 51%, with an average of 40%. The average overall mean phase difference was 63° (range 52–67°), with an average amplitude weighted difference of 31° (range 24–37°). These results are due to the fact that there are many reflections of small amplitude and random phase which contribute strongly to the unweighted phase residuals.

Distortions in the crystal lattice are evident in the micrographs and limit the resolution of the image. Real-space correlation averaging with unbending or Fourier averaging after rotational alignment with unbending has been applied to the images to see to what extent the distortions can be removed and agreement with the x-ray data improved. The data shown in Table 1 indicate that the images that benefit significantly from these procedures are the most distorted. There is little difference in the improvement obtained between the two different lattice straightening methods. Wilson plots of the distortion-corrected EM amplitudes reveal a modest improvement in resolution, which is still, however, less than that of the x-ray crystallographic data. Correspondingly, a density map derived from the distortion-corrected structure factors appears generally similar to that produced from the uncorrected data (Fig. 2 *a*).

Next, the *pmg* symmetry of the images was used as a constraint to correct the phases and average the two independent measurements of each unique reflection. A modest improvement of the phases is seen, but the amplitudes are still in poor agreement. Unlike the x-ray map, however, the crossover regions appear to have four distinct nodes of high density, and the filament strands are surrounded by fringes of weak density (Fig. 2 *b*).

The fringes in the EM map are due to the down weighting of the very low resolution terms as a result of the CTF (for review see Erikson and Klug, 1971). Given the amount of underfocus, the relative contributions of phase and amplitude contrast, and other microscope parameters, it is possible to calculate "corrected" amplitudes. The underfocus was estimated to be 7,000 Å by measurement of Thon rings of areas of carbon adjacent to the crystals in the micrographs, and was chosen so that the first zero in the transfer function was outside the resolution range containing any significant diffraction in the transformed images. The fraction that amplitude

FIGURE 1 (*a–c*) The [0kl] view of the tropomyosin Bailey crystal mesh. (*a*) Cryoelectron microscopy image of an unstained crystal fragment embedded in vitreous ice. Micrograph taken at 7,000 Å underfocus. The inset is an area of a different crystal showing separation of the tropomyosin filaments; the micrograph was taken at the same defocus and electron dose rate. (*b*) Electron micrograph of a crystallite stained with 1% uranyl acetate. Micrograph taken at 3,000 Å underfocus. (*c*) Diagram of four contiguous unit cells of the [0kl] view determined by x-ray diffraction. The kite-shaped net of this projection is apparent from all three methods. (*d–f*) Diffraction patterns from tropomyosin crystals. (*d*) Computed diffraction pattern from the image of the ice-embedded crystal shown in (*a*). The pattern extends to 18 Å resolution. (*e*) Computed diffraction pattern from the low dose image of a negatively stained crystal shown in (*b*). The pattern extends to 30 Å resolution. (*f*) X-Ray precession photograph of the same crystal view extending to 15 Å resolution.

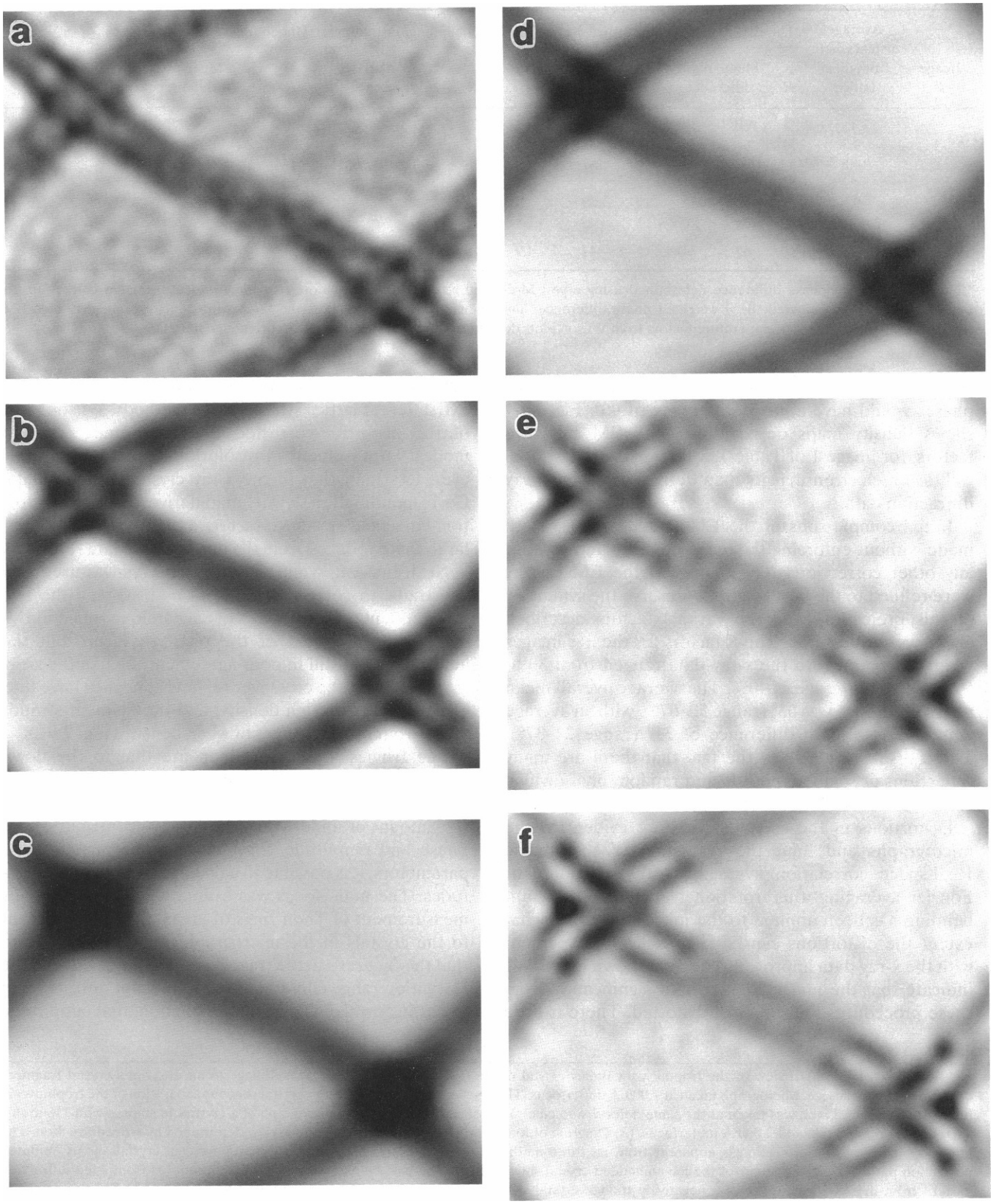
a
b
c
d
e
f

contrast (the cosine term) contributes to the CTF was obtained empirically by varying it from 0.0 to 0.2 in small increments to minimize the low resolution R factor; the optimum value was always near 0.06. This value is similar to that found using pairs of defocused images (Toyoshima and Unwin, 1988). Using this correction, the stronger low resolution amplitudes were brought into reasonable agreement with the x-ray amplitudes. In a map derived from these structure factors the fringes have been eliminated, but the structural features discernible are limited because the higher order reflections are now weighted less strongly relative to the low resolution terms (Fig. 2 *c*).

This difference in resolution between the CTF-corrected micrographs and the x-ray-derived images can be partially compensated for by applying an inverse Debye-Waller temperature factor to enhance the high resolution terms. A Wilson plot was constructed for each of the images (see Fig. 3 for image 1) and the Debye-Waller factor, B, determined from the plot. A map produced after applying a temperature factor with a value of 0.6 times B to the EM structure factors is now very similar to the x-ray map, although it is noisier and slightly lower in resolution (Fig. 2 *d*). As in the x-ray map, the crossover regions have a V-shaped band of high density with a small node opposite the band. A protein dense region extends into the short arms of the mesh at the tropomyosin head-to-tail overlap. Attempts to increase the resolution further with larger temperature factors only added more Fourier ripples.

To test whether phases from the cryo-EM images could be applied directly to the x-ray crystallographic amplitudes to produce an accurate map, a hybrid map was calculated using the phases from the structure factors of image 1 with the x-ray amplitudes. It is apparent that the phases are accurate enough to give a clearly interpretable map, although the noise level is slightly higher than in the refined x-ray structure (Fig. 2 *e*).

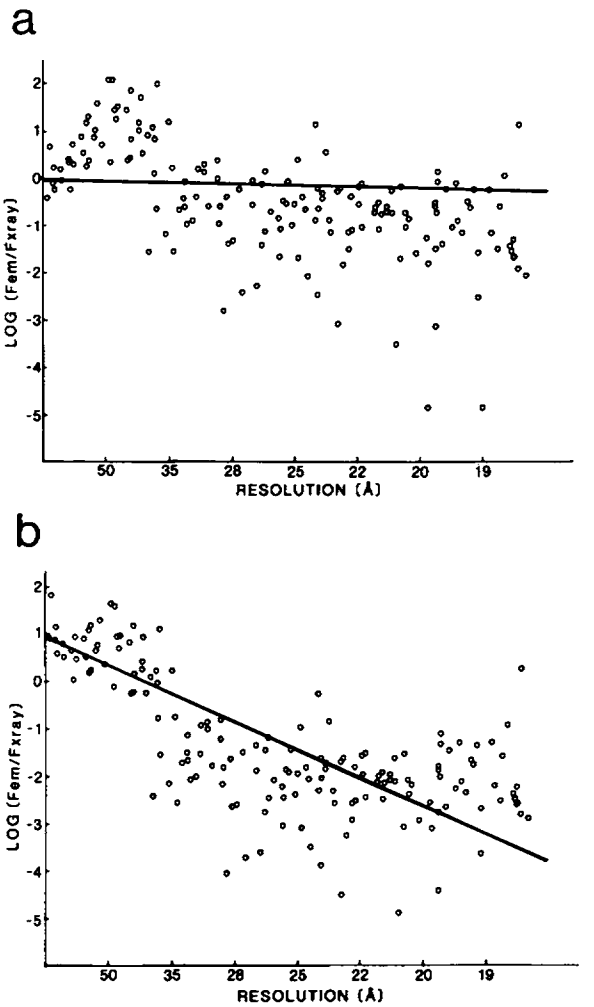

FIGURE 3 Wilson plots for image 1. The log of the ratio of the x-ray intensities to the square of the EM-derived amplitudes is plotted versus $\sin^2\theta/\lambda^2$. The x-axis is labeled in intervals of resolution ($d = \lambda/2\sin\theta$). (*a*) The EM amplitudes were extracted after lattice straightening and *pmg* symmetry imposed. (*b*) EM amplitudes used are those from *a* after correcting for the CTF at 7,000 Å underfocus. The Debye-Waller temperature factor was initially determined from the slope of the line in *b*.

Tropomyosin/troponin cocrystals

In the preparation that gave the best images, the tropomyosin/troponin Bailey cocrystals embedded in ice were somewhat larger than the pure tropomyosin crystals (~1,000 unit cells per micrograph). It is apparent from the unprocessed image of a cocrystal that not all of the troponin binding sites are occupied (Fig. 4 *a*). The

FIGURE 2 Density maps of a single unit cell of the tropomyosin crystal. (*a–d*) Maps produced from structure factors to 18 Å from cryo-EM image 1. (*a*) Fourier average. (R = 51, weighted mean phase difference (WMPD) = 34°). (*b*) After lattice straightening and *pmg* symmetry imposed (R = 46, WMPD = 30.6°). (*c*) Map from structure factors in *b* after correcting for the CTF at 7,000 Å underfocus (R = 26, WMPD = 30.6°). (*d*) Map produced from the structure factors in *c* after applying Debye-Waller temperature factor (the temperature factor was first multiplied by 0.6 before being applied to the EM amplitudes to enhance the higher order terms without adding excessive noise to the solvent region) (R = 20, WMPD = 7.8°). (*e*) Hybrid map produced using amplitudes from x-ray diffraction and phases from cryoelectron microscopy. (*f*) Electron density map from structure factors derived from x-ray diffraction.

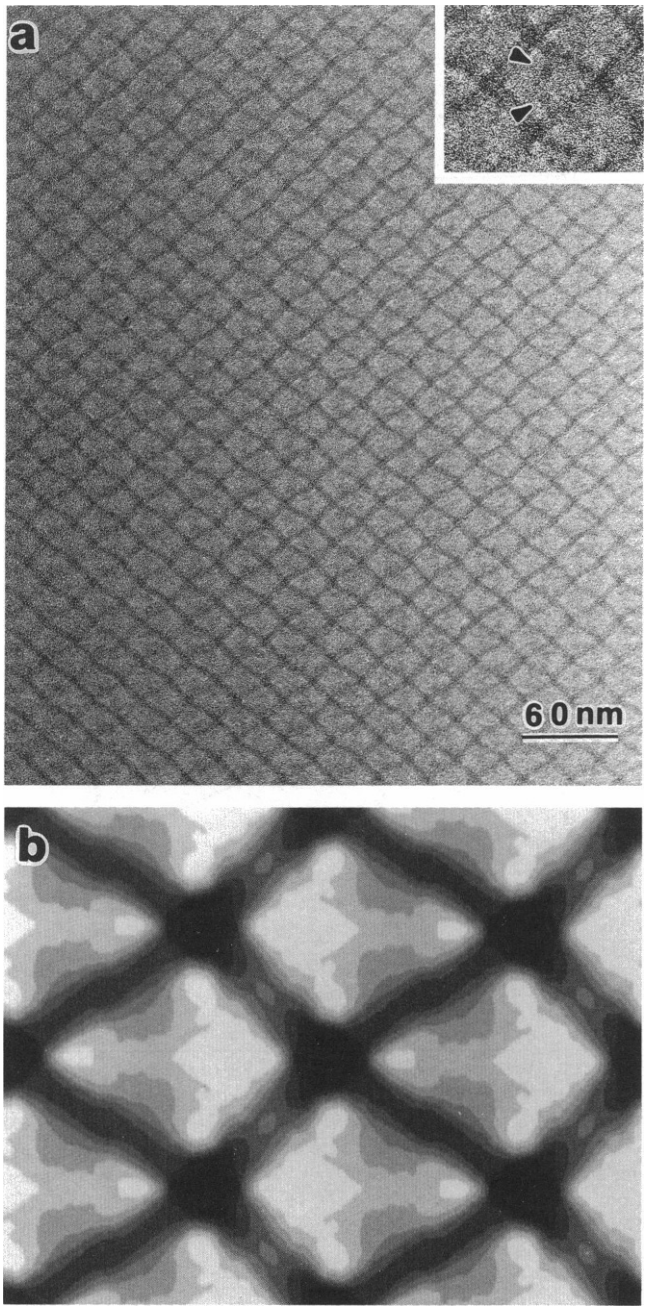

FIGURE 4 Tropomyosin/troponin cocrystals. (*a*) Image of an unstained cocrystal in vitreous ice taken at 8,000 Å underfocus. The inset shows a unit cell with two troponin heads visible (*arrows*). (*b*) Density map at 20 Å resolution showing four contiguous unit cells, produced from averaging four correlation averages. The head region of troponin is located near the center of the long arms.

kite-shaped net is seen with the troponin head region visible as a globular area of extra density at the center of the long arms. The head region can be more easily seen as bands of extra density by looking parallel to the vertical axis at a small angle from the page. Correlation averaging was therefore used to produce a map at 20 Å resolution from four images (Fig. 4 *b*). After processing, the density of the troponin head region is still weak relative to the tropomyosin lattice, and appears disordered. The center of mass of the head has a length of roughly 40 Å. The arms of the net are ~10–15 Å thicker than those of pure tropomyosin along the entire length except for the center of the short arms. This finding suggests that in this projection of the cocrystal the tail portion of the troponin T molecule appears to be closely associated with the tropomyosin filaments.

DISCUSSION

The tropomyosin Bailey crystal is an excellent system for analysis by coordinated electron microscopy and x-ray diffraction. One projection of the lattice is easily visualized by electron microscopy, and negatively stained images of this view provided essential information for the solution of the crystal structure. However, just as technical problems were encountered in the x-ray diffraction studies (Caspar et al., 1969; Phillips et al., 1986), certain features of the crystals used for this initial cryo-EM study presented some difficulties. The large unit cell size, as well as the small crystalline areas in any field limited our ability to obtain good electron diffraction intensities at higher resolutions than the images. The amplitudes are therefore estimated by correcting the structure factors extracted from computed diffraction patterns for the CTF and the disorder present in the images. Although the amount of underfocus used for CTF corrections was not refined, corrections applied at defoci of ±0.1 μm do not significantly change the resulting maps. The amplitudes of the extracted structure factors are weak relative to the x-ray amplitudes and fall off more markedly at resolutions >40 Å; a Debye-Waller temperature factor was therefore applied to increase these amplitudes. This effect may be due to several factors, including specimen movement, disorder in the crystal lattice, the small number of unit cells averaged, and differences in protein/solvent contrast for x-ray versus electron scattering (see Henderson and Glaeser, 1985). Improvements in specimen preparation, data collection, and image processing decreased this effect significantly for purple membrane (Baldwin et al., 1988). Similarly, improvements in specimen preparation to yield large, thin tropomyosin Bailey crystals should produce higher resolution data.

The density map of the tropomyosin Bailey crystal derived from the processed cryo-EM images shows excellent agreement with the corresponding projection of the three-dimensional structure determined from

x-ray crystallography. The unit cell parameters, and the width and run of the filaments are the same; moreover, the woven appearance of the filaments is evident at the crossover regions of each map. The head-to-tail overlap of tropomyosin molecules in a filament was visualized in three dimensions to 15 Å by x-ray diffraction (Phillips et al., 1986); it is also discernible in the 18 Å map from the processed cryo-EM images. The pitch of the coiled coil was found to be ~140 Å (corresponding to three turns per molecular length) in the x-ray study. It was not possible to obtain a good estimate of the pitch length from the electron microscopy data in this study because of the limited resolution and the fact that only one projection was available. The signal-to-noise ratios of the higher order reflections are greater in the x-ray map of this projection than the map derived from cryo-EM, primarily because there are many more unit cells in the former case (10^{12} versus 200 for average-sized crystals). The contrast of the maps is also somewhat different due to the different scattering cross-sections for electrons and x-rays for C, N, and O. Despite the limitations encountered in the present study, however, the results show that considerable structural detail in these highly hydrated crystals can be obtained from relatively simple, straightforward methods of cryoelectron microscopy and image processing.

Our first views of tropomyosin/troponin cocrystals by this method are promising: troponin is visible even in the unprocessed micrographs. X-Ray crystallographic analysis at 17 Å resolution of cocrystals of tropomyosin containing whole troponin or fragments of troponin T showed that the NH_2-terminal portion of troponin T spans the head-to-tail joint of the tropomyosin filaments; the troponin head region appeared to bind between residues 150–180 of tropomyosin (White et al., 1987). Little density, however, could be detected for troponin T between the crossover region and the troponin head. In the present study, processed images of the cocrystals also indicate that one end of troponin T spans the tropomyosin end-to-end overlap region, but troponin T appears to be closely associated along its entire length with the tropomyosin filament. Electron microscopy of the tropomyosin/troponin T "double diamond" cocrystals (Carr et al., 1988; Cabral-Lilly, D., L. S. Tobacman, J. P. Mehegan, and C. Cohen, manuscript in preparation) also shows that the entire tail portion of troponin T appears to lie in contact with the tropomyosin filaments. The findings from the x-ray analysis may be accounted for, in part, by the relatively large molecular motions in the Bailey cocrystal lattice. In the cryo-EM images analyzed thus far, although the troponin head region is visible, its density is still relatively weak, due primarily to partial occupancy and conformational variability: molecular motions may have "frozen" the head region in slightly different conformations leading to a disordered appearance. Correlation averaging techniques can compensate in part for these problems. Improvements in crystal preparations to obtain large, well-ordered arrays should significantly improve these maps. These studies provide the basis for analysis of the calcium-dependent conformational changes in the tropomyosin/troponin regulatory switch.

We thank Drs. Timothy Baker, Thomas Tibbitts, and Michael Schmid for providing programs used to image process the cryo-EM micrographs.

This work was supported by National Institutes of Health (NIH) grants HL-07682 (D. Cabral-Lilly), AR17346 (C. Cohen), AR32764 (G. N. Phillips), and a grant from the Muscular Dystrophy Association (C. Cohen). Part of this work was done during the tenure of a research fellowship to D. Cabral-Lilly from the American Heart Association, Massachusetts Affiliate, Inc. G. E. Sosinsky was a Charles A. King Trust Fellow from The Medical Foundation of Boston. Funds to purchase and maintain the computer system were obtained from a Shared Instrumentation grant 1-S10-RR04671-01 awarded to David J. DeRosier by NIH. Funds to purchase and maintain the Philips EM420T transmission electron microscope were obtained from a Shared Instrumentation grant 1-S10-RR02464-01 awarded to C. Cohen by NIH.

Received for publication 1 June 1990 and in final form 10 December 1990.

REFERENCES

Baldwin, J. M., R. Henderson, E. Beckmann, and F. Zemlin. 1988. Images of purple membrane at 2.8 Å resolution obtained by cryo-electron microscopy. *J. Mol. Biol.* 202:585–591.

Carr, H. J., E. J. O'Brien, and E. P. Morris. 1988. Structure of tropomyosin-troponin T cocrystals. *J. Muscle Res. Cell Motil.* 9:384–392.

Caspar, D. L. D., C. Cohen, and W. Longley. 1969. Tropomyosin: crystal structure, polymorphism and molecular interactions. *J. Mol. Biol.* 41:87–107.

Chiu, W. 1986. Electron microscopy of frozen hydrated biological specimens. *Annu. Rev. Biophys. Biophys. Chem.* 15:237–257.

Cohen, C., D. L. D. Caspar, D. A. D. Parry, and R. M. Lucas. 1971. Tropomyosin crystal dynamics. *Cold Spring Harbor Symp. Quant. Biol.* 36:205–216.

Dubochet, J., M. Adrian, J. J. Chang, J. C. Homo, J. Lepault, A. W. McDowall, and P. Schultz. 1988. Cryo-electron microscopy of vitrified specimens. *Q. Rev. Biophys.* 21:129–228.

Erickson, H. P., and A. Klug. 1971. Measurement and compensation of defocusing and aberrations by Fourier processing of electron micrographs. *Philos. Trans. R. Soc. Lond. B Biol. Sci.* B261:105–118.

Glaeser, R. M. 1985. Electron crystallography of biological macromolecules. *Annu. Rev. Phys. Chem.* 36:243–275.

Greaser, M. L., and J. Gergely. 1973. Purification and properties of the components from troponin. *J. Biol. Chem.* 248:2125–2133.

Greaser, M. L., M. Yamaguchi, and G. Vanderkooi. 1977. Crystal forms of α_2-tropomyosin. *J. Mol. Biol.* 116:883–890.

Henderson, R., and R. M. Glaeser. 1985. Quantitative analysis of image contrast in electron micrographs of beam-sensitive crystals. *Ultramicroscopy.* 16:139–150.

Henderson, R., J. M. Baldwin, K. H. Downing, J. Lepault, and F. Zemlin. 1986. Structure of purple membrane from *Halobacterium halobium:* recording, measurement and evaluation of electron micrographs at 3.5 Å resolution. *Ultramicroscopy.* 19:147–178.

Henderson, R., J. M. Baldwin, T. A. Ceska, F. Zemlin, E. Beckmann, and K. H. Downing. 1990. A model for the structure of bacteriorhodopsin based on high resolution electron cryo-microscopy. *J. Mol. Biol.* 213:899–929.

Higashi, S., and T. Ooi. 1968. Crystals of tropomyosin and native tropomyosin. *J. Mol. Biol.* 34:699–701.

Jap, B. K., K. H. Downing, and P. J. Walian. 1990. Structure of PhoE porin in projection at 3.5 Å resolution. *J. Struct. Biol.* 103:57–63.

Jeng, T. W., R. A. Crowther, G. Stubbs, and W. Chiu. 1989. Visualization of alpha-helices in tobacco mosaic virus by cryo-electron microscopy. *J. Mol. Biol.* 205:251–257.

Lehrer, S. S. 1975. Intramolecular crosslinking of tropomyosin via disulfide bond formation: evidence for chain register. *Proc. Natl. Acad. Sci. USA.* 72:3377–3381.

Phillips, G. N., Jr., E. E. Lattman, P. Cummins, K. Y. Lee, and C. Cohen. 1979. Crystal structure and molecular interactions of tropomyosin. *Nature* (*Lond.*). 278:413–417.

Phillips, G. N., Jr., J. P. Fillers, and C. Cohen. 1980. Motions of tropomyosin. Crystal as metaphor. *Biophys. J.* 32:485–502.

Phillips, G. N., Jr., J. P. Fillers, and C. Cohen. 1986. Tropomyosin crystal structure and muscle regulation. *J. Mol. Biol.* 192:111–131.

Phillips, G. N., Jr., C. Cohen, and M. Stewart. 1987. A new crystal form of tropomyosin. Preliminary x-ray diffraction analysis. *J. Mol. Biol.* 195:219–223.

Salmon, E. D., and D. DeRosier. 1981. A surveying optical diffractometer. *J. Microsc.* (*Oxf.*). 123:239–247.

Sosinsky, G. E., T. S. Baker, D. L. D. Caspar, and D. A. Goodenough. 1990. Correlation analysis of gap junction lattice images. *Biophys. J.* 58:1213–1226.

Stewart, M. 1984. Crystalline sheets of tropomyosin. *J. Mol. Biol.* 174:231–238.

Toyoshima, C., and N. Unwin. 1988. Contrast transfer for frozen-hydrated specimens: determination from pairs of defocused images. *Ultramicroscopy.* 25:279–292.

White, S. P., C. Cohen, and G. N. Phillips, Jr. 1987. Structure of co-crystals of tropomyosin and troponin. *Nature* (*Lond.*). 325:826–828.

Wilson, A. J. C. 1949. The probability distribution of x-ray intensities. *Acta Cryst.* 2:318–321.